# SUMOylation restrains ACE2 degradation through TOLLIP-mediated selective autophagy to facilitate the host susceptibility to SARS-CoV-2 infection

**Jun Cui** ( cuij5@mail.sysu.edu.cn )
Sun Yat-sen University
**Shouheng Jin**
Sun Yat-sen University https://orcid.org/0000-0002-2728-2859
**Xing He**
Sun Yat-sen University
**Ling Ma**
Sun Yat-sen University
**Meng Lin**
Sun Yat-sen University
**Sihui Cai**
Sun Yat-sen University
**Lu Wei**
Sun Yat-sen University
**Zhiyao Zhao**
The First Affiliated Hospital of Guangzhou Medical University
**Yaoxing Wu**
Sun Yat-sen University
**Lin Sun**
Sun Yat-sen University
**Li Chun-Wei**
Sun Yat-sen University
**Yong Zhao**
Sun Yat-sen University
**Zhou Songyang**
Verna and Marrs Mclean Department of Biochemistry and Molecular Biology, Baylor College of Medicine, One Baylor Plaza, Houston, TX
**Ke Peng**
Wuhan Institute of Virology
**Jincun Zhao**
The First Affiliated Hospital of Guangzhou Medical University

**Article**

**Keywords:** COVID-19 Pandemic, Host-virus Dependencies, Proteome-wide Protein Interaction Analysis, Antiviral Therapy

**Posted Date:** March 31st, 2021

**DOI:** https://doi.org/10.21203/rs.3.rs-358319/v1

# Abstract

Severe acute respiratory syndrome coronavirus 2 (SARS-CoV-2) is the causative agent of the ongoing coronavirus disease 2019 (COVID-19) pandemic. Alongside investigations into the virology of SARS-CoV-2, understanding the host–virus dependencies are vital for the identification and rational design of effective antiviral therapy. Here, we report the dominant SARS-CoV-2 entry receptor, ACE2, conjugates with small ubiquitin-like modifier 3 (SUMO3) through a proteome-wide protein interaction analysis. We further demonstrate that E3 SUMO ligase PIAS4 prompts the SUMOylation and stabilization of ACE2, whereas deSUMOylation enzyme SENP3 reverses this process. Conjugation of SUMO3 with ACE2 at lysine (K) 187 hampers the K48-linked ubiquitination of ACE2, thus suppressing its subsequent cargo receptor TOLLIP-dependent autophagic degradation. Pharmacological intervention of ACE2 SUMOylation blocks the entry of SARS-CoV-2 and viral infection-triggered immune responses. Collectively, our findings suggest selective autophagic degradation of ACE2 orchestrated by SUMOylation and ubiquitination can be targeted to future antiviral therapy of SARS-CoV-2.


# Introduction

The ongoing coronavirus disease 2019 (COVID-19) pandemic caused by severe acute respiratory syndrome coronavirus 2 (SARS-CoV-2) infection, has posed an extraordinary threat to global health and economy[1, 2]. Coronaviruses are a diverse group of enveloped viruses infecting many different vertebrates, and they can cause mild to severe respiratory and intestinal infections in humans[3]. Coronavirus tropism is predominantly dependent on the interaction between trimeric coronavirus spike (S) glycoproteins and their matching host receptors. The S protein of SARS-CoV-2 (SARS-2-S) can be cleaved into the S1 (SARS-2-S1) and S2 (SARS-2-S2) subunits during viral entry, which is essential for receptor recognition and membrane fusion. Angiotensin-converting enzyme 2 (ACE2) has been demonstrated as a host cell target receptor of SARS coronavirus[4, 5]. Owing to the high sequence similarity between S proteins of SARS-CoV and SARS-CoV-2, researchers have uncovered that SARS-CoV-2 uses ACE2 as its dominated entry receptor and binding of SARS-CoV-2 to ACE2 occurs through the C-terminal domain (also named as the receptor-binding domain (RBD)) of SARS-2-S1[6, 7]. Therefore, antibodies, peptides and small compounds targeting ACE2 can be applied to the treatment of SARS-CoV-2 infection[8-10]. However, the precise regulation of ACE2 during viral infection remains largely unclear.

Autophagy is a conserved eukaryotic intracellular degradation system to sequester cytoplasmic components into autophagosomes, which follows by fusing with lysosomes to degrade the captured substrates for recycle[11, 12]. Emerging evidence indicates that substrates are engulfed into autophagosomes in a selective manner which is mediated by autophagy cargo receptors such as p62/SQSTM1, nuclear dot protein 52 (NDP52), NBR1 (neighbor of BRCA1), and Toll interacting protein (TOLLIP)[13, 14]. These receptor proteins tackle ubiquitinated substrates through their ubiquitin-binding domains and are linked with autophagosomes via the light chain 3 (LC3)-interacting regions[15]. So far, which linkage types of poly-ubiquitin chains can target to special cargo for autophagic degradation are

yet to be fully characterized[16], and understanding of the underlying mechanism of selective autophagy prompts developments of autophagy-modulating medicine with cargo selectivity[17].

Reversible post-translational modification by the small ubiquitin-like modifier (SUMO) plays a crucial role in ensuring a highly dynamic regulation of cellular functions, such as protein stability, localization, interactions, as well as the activity of substrates[18, 19]. In mammals, SUMOylation entails an enzymatic cascade mediated by the E1 SUMO-activating enzyme (SAE), the E2-conjugating enzyme, UBC9, and a limited set of E3 SUMO ligases[20]. Conversely, SUMOylation is able to be quickly reversed by SUMO/Sentrin specific proteases (SENPs)[21]. In this study, we found E3 SUMO ligase PIAS4 promotes the conjugation of SUMO3 with ACE2, whilst deSUMOylating enzyme SENP3 decreases the SUMOylation level of ACE2. The covalent association of SUMOylation of ACE2 dampens the K48-linked ubiquitination of ACE2 at lysine (K) 187, thereby hindering TOLLIP-ACE2 interaction along with the degradation of ACE2 through selective autophagy. Given the vital role of the ACE2 receptor in the early stages of viral entry, we prick the bubble that loss of SUMOylation reduces viral entry by sequestering ACE2 through autophagic degradation. Our findings illustrate that SUMOylation restrains the degradation of ACE2 receptor through TOLLIP-mediated selective autophagy to facilitate the host susceptibility against SARS-CoV-2 infection, which might be a potential therapeutic target of COVID-19.

# Results

### ACE2 undergoes SUMO modification.

To delineate the large-scale proteomic landscape of ACE2 interaction and regulation, we adopted mass spectrometry (MS) using ACE2 as a bait and identified 773 ACE2-ineracting proteins (Supplementary Table 1), among which we discovered a portion associated with SUMOylation by means of Gene Ontology (GO) enrichment analysis towards biological process, one of three major GO analysis terms (Fig. 1a). Protein conjugation with SUMO (Fig. 1b), has attracted considerable attention owing to its indispensable roles in mammalian cells[21]. We immunoprecipitated SUMO from cellular extracts following denaturing conditions to avoid the isolation of protein complexes, and detected high apparent band of ACE2 in the SUMO2/3/4 immunoprecipitates (Fig. 1c). SUMO2, SUMO3 and SUMO4 are virtually identical[18], and there is no commercial antibody to be capable of distinguishing them. To figure out which type of SUMO could be conjugated with ACE2, we next co-overexpressed different types of SUMO with ACE2 and observed that ACE2 specifically linked with SUMO3. Moreover, the amount of SUMOylated ACE2 was increased following UBC9 overexpression (Fig. 1d). Due to the critical C-terminal di-Gly motif of SUMO3 in the attachment to substrates, the conjugation of ACE2 was totally abrogated within the mutant form of SUMO3 (SUMO3 GG/AA) (Fig. 1e). Furthermore, we observed that cells treated with ML-792, the selective inhibitor of SAE/SUMO (Fig. 1f), exhibited dramatically lower appearance of SUMOylated ACE2 (Fig. 1g-i). Bioinformatics analysis of ACE2 predicted five potential SUMO-conjugation consensus motifs (Fig. 1j and Extended Data Fig. 1a,b), and we generated the ACE2 mutants bearing single lysine (K) to arginine (R) substitution in every potential SUMOylation site for *in vivo* SUMOylation assay. Our results

showed only K187R ACE2 mutant displayed reduced SUMOylation (Fig. 7k), suggesting that K187 functions as a critical SUMOylation site of ACE2. Taken together, all these results revealed that ACE2 undergoes SUMO3 conjugation and K187 contributes to this modification.

## PIAS4 targets ACE2 for SUMOylation-mediated stabilization.

Next, we sought to determine which SUMO E3 ligase is responsible for the SUMOylation of ACE2 and found that Myc-PIAS4 interacted with HA-ACE2 (Fig. 2a). We used a specific antibody against ACE2 (anti-ACE2) to immunoprecipitate ACE2-associated protein complexes and found the endogenous association between ACE2 and PIAS4 in Calu-3 cells and human nasal epithelial progenitor cells (hNEPCs) (Fig. 2b,c). We further observed the co-localization of ACE2 and PIAS4 by confocal microscopy (Fig. 2d,e). To study the potential physiological role of ACE2-PIAS4 interaction, we co-expressed Flag-ACE2 and Myc-PIAS4 in 293T cells and found that ACE2 protein amount positively correlated with PIAS4 protein amount (Extended Data Fig. 2a). We also examined the *ACE2* mRNA levels in the same cells and found the abundances of *ACE2* mRNA did not altered with increased expression of PIAS4 (Extended Data Fig. 2b). To determine whether PIAS4 affects ACE2 stability via SUMOylation, we analyzed the amount of SUMOylated ACE2 with the existence of PIAS4, and found that PIAS4 promotes the stabilization of ACE2 through SUMOylation (Extended Data Fig. 2c).

We further evaluated whether SUMOylation influences the turnover of ACE2 and observed that the ACE2 protein levels but not the corresponding mRNA levels were gradually decreased upon ML-792 treatment in a dose-dependent manner (Fig. 2f,g and Extended Data Fig. 2d). Consistently, we obtained a similar result with the treatment of another inhibitor of SUMOylation 2-D08, which prevents transfer of SUMO from the UBC9-SUMO thioester to the substrate (Fig. 2h-j and Extended Data Fig. 2e). We then examined the ACE2 protein abundances in hNEPCs and observed that both ML-792 and 2-D08 treatments attenuate the protein stability of ACE2 (Fig. 2k,l). Moreover, we found that 2-D08-induced degradation of ACE2 was almost abolished when K187 is mutated (Fig. 2m), and PIAS4 lost the ability to promote the SUMOylation and stabilization of ACE2 K187 mutant (Fig. 2n). Taken together, our findings indicated that PIAS4 mediates the SUMOylation of ACE2 at K187 to promote its stabilization.

## PIAS4 suppresses the autophagic degradation of ACE2.

There are three major systems which eukaryotic cells used to control protein degradation: the proteasome, lysosome and autolysosome pathways[16, 22]. We next identified which degradation system dominantly mediates the stability of ACE2, and found the up-regulation of Flag-ACE2 protein level mediated by PIAS4 could be abrogated by the autophagy inhibitor 3-methyladenine (3-MA) or autolysosome inhibitor bafilomycin A1 (Baf A1), but not the proteasome inhibitor MG132 (Fig. 3a), suggesting that PIAS4 shut down the autophagic degradation of ACE2. We next found that the autophagic degradation of ACE2 was potentiated by *PIAS4* depletion (Fig. 3b). In addition, the stabilization of ACE2 triggered by PIAS4 was almost abrogated in *BECN1* and *ATG5* knockout (KO) cells, in which the autophagy is significantly impaired (Fig. 3c). We also observed the degradation of ACE2

upon rapamycin treatment and starvation-induced autophagy activation under Earle's balanced salt solution (EBSS) culture condition (Fig. 3d,e). Additionally, the autophagic degradation of ACE2 was totally blocked in the presence of Baf A1, and the level of p62 (an autophagy substrate) displayed a similar expression pattern (Extended Data Fig. 3a). We next assessed whether PIAS4 promotes the SUMOylation of ACE2 at K187 to prevent its autophagic degradation, and observed that the ACE2 turnover rates were largely reduced by K187R mutation upon autophagy activated conditions (Fig. 3f,g and Extended Data Fig. 3b,c). Collectively, these results suggested that PIAS4-mediated SUMOylation attenuates the degradation of ACE2 through autophagy.

**PIAS4 suppresses the interaction between ACE2 and TOLLIP for selective autophagic degradation.**

Increasing evidence suggested that cargo receptors play essential roles in delivering substrates to the autophagosome for selective degradation[14, 16]. We found that ACE2 mainly associated with TOLLIP rather than other cargo receptors (Fig. 4a), and further detected the endogenous association between ACE2 and TOLLIP (Fig. 4b,c). Confocal imaging demonstrated that ACE2 colocalized with TOLLIP, and the ACE2-TOLLIP association increased considerably at 1 hr upon starvation treatment (Fig. 4d,e and Extended Data Fig. 4a). We next knocked down the expression of *TOLLIP*, and observed that the autophagic degradation of ACE2 was abolished in *TOLLIP* depletion cells (Fig. 4f and Extended Data Fig. 4b). Additionally, we found that PIAS4 disrupted the interaction between ACE2 and TOLLIP (Extended Data Fig. 4c). *PIAS4* knockdown dramatically enhanced the interaction of endogenous ACE2 and TOLLIP (Fig. 4g). In addition, PIAS4 failed to block the autophagic degradation of ACE2 in *TOLLIP* depletion cells (Fig. 4h). All together, these results indicated that PIAS4 disrupts the interaction between ACE2 and the cargo receptor TOLLIP for selective autophagic degradation.

**SUMOylation deceases the K48-linked ubiquitination of ACE2.**

As SUMOylation prompted the stabilization of ACE2, we next examined if SUMOylation inhibits the recognition of ACE2 by cargo receptor TOLLIP, and found that interaction between ACE2 and TOLLIP was enhanced after 2-D08 treatment (Fig. 5a). TOLLIP contains a Tom1-binding domain (TBD) (aa 1–54), a phospholipid-binding C2-domain harboring two putative LC3/Atg8-interacting motifs (aa 55–181), and a ubiquitin-binding CUE domain (aa 219–274) (Fig. 5b). To further elucidate the mechanism of ACE2 recognition, we generated TOLLIP R78A or M240A/F241A, L267A/L268A (CUE domain mutant) constructs, which inhibit the binding of TOLLIP to phosphatidylinositol 3-phosphate (PI3P) and PI(4,5)$P_2$ or ubiquitin, respectively[23, 24]. Since TOLLIP CUE mutants cannot interact with ACE2 (Fig. 5c), we hypothesized that ubiquitin chains on ACE2 may serve as a recognition signal for subsequent TOLLIP-dependent degradation. We performed MS analysis to investigate the ubiquitination of purified ACE2, and identified a specific K48-linked poly-ubiquitin peptide (Fig. 5d). The MS findings were further validated in co-immunoprecipitation studies and the K48-linked ubiquitination of ACE2 was remarkably elevated upon 2-D08 treatment (Fig. 5e). We next employed the plasmid expressing HA-K48R-Ub, which features a K48 to R48 mutation, and observed that the ubiquitination of ACE2 with other linkage type was not influenced

after 2-D08 treatment (Extended Data Fig. 5). Taken together, these results indicated that K48-linke poly-ubiquitin chains on ACE2 might be a recognition signal for TOLLIP.

To further study whether SUMOylation dampens the K48-linked ubiquitination of ACE2, we first studied the role of PIAS4 in ACE2 ubiquitination and observed that the K48-linked ubiquitination of ACE2 was increased by *PIAS4* silencing (Fig. 5f). In addition, we found that the K48-linked ubiquitination of ACE2 K187R mutant was barely observed, no matter PIAS4 is expressed or not (Fig. 5g), suggesting K187 might be an essential site for both SUMOylation and K48-linked ubiquitination of ACE2. The ubiquitination modification of ACE2 at K187 was further demonstrated by MS analysis (Fig. 5h). The association with TOLLIP was significantly disrupted when K187 of ACE2 was mutated (Fig. 5i) and K187R had a slower turnover rates (Fig. 5j,k). Taken together, our findings suggested that K187 on ACE2 functions as a critical K48-linked ubiquitination site for TOLLIP recognition.

**DeSUMOylation by SENP3 promotes autophagic recognition and degradation of ACE2.**

ACE2 serves as the main receptor for the envelope coated by spike protein of SARS-CoV-2. To better understand the dynamic ACE2 SUMOylation in the initial attachment of SARS-CoV-2, we studied the roles of deSUMOylation enzymes in the infection of SARS-CoV-2 S pseudotyped virus. First, we transduced a human alveolar basal epithelial carcinoma cell line (A549) that constitutively expresses ACE2 with an all-in-one lentiviral vector containing Cas9, guide RNAs from 7 SENP deSUMOylating enzymes, and a puromycin resistance gene. We then selected with puromycin so that only infected cells (A549-ACE2) remained. After puromycin selection was completed, we cultured the cells for 9 days to ensure protein depletion after CRISPR gene targeting. Next, we infected the selected A549-ACE2 cells with SARS-CoV-2 S pseudotyped virus (Fig. 6a), and found that *SENP3* depletion dramatically enhanced the SARS-CoV-2 S pseudotyped virus infection by luciferase assay (Fig. 6b), implying SENP3 may work as a negative regulator for SARS-CoV-2 invasion. We focused on SENP3 and verified the interaction between SENP3 and ACE2 (Fig. 6c,d and Extended Data Fig. 6a). SENP3 overexpression promoted the ACE2 degradation, whereas the protein abundances of ACE2 were up-regulated by *SENP3* deficiency (Fig. 6e and Extended Data Fig. 6b).

We sought to determine whether SENP3 potentiates the recognition and degradation of ACE2 and observed that the interaction between ACE2 and TOLLIP was suppressed in *SENP3* deficient Calu-3 cells (Fig. 6f). Consistently, SENP3-mediated ACE2 degradation was abrogated in *TOLLIP* deficient cells (Fig. 6g). In addition, the SUMO3 modification of ACE2 was elevated, while the K48-linked ubiquitination of ACE2 was decreased by *SENP3* depletion (Fig. 6h). Immunofluorescence analysis revealed that the K48-linked ubiquitination of ACE2 was enhanced in *SENP3* deficient cells (Fig. 6i and Extended Data Fig. 6c). Together, our results demonstrated that SENP3 restrains the SUMOylation of ACE2, which subsequently promotes its K48-linked ubiquitination and TOLLIP-dependent autophagic degradation.

**Dynamic SUMOylation of ACE2 has an impact on the host susceptibility to SARS-CoV-2 infection.**

To understand the physiological role of TOLLIP-mediated selective autophagy of ACE2 in the SARS-CoV-2 infection, we performed immunofluorescence analysis of the lung from transgenic hACE2 mice and observed that TOLLIP-ACE2 interaction was largely elevated upon SARS-CoV-2 infection (Fig. 7a,b). We then depleted the expression of *TOLLIP* and observed that the ACE2 protein abundance and the SARS-CoV-2 proliferation were significantly increased (Fig. 7c). Consistently, the SARS-CoV-2 infection-induced innate immune responses were reduced in *TOLLIP* deficient cells (Fig. 7d). Our results indicated that TOLLIP-directed autophagic degradation of ACE2 restricts the entry of SARS-CoV-2 to host cells. To further examine the role of ACE2 SUMOylation in SARS-CoV-2 infection, we collected the poly-A enriched RNA from the SARS-CoV-2-infected Calu-3 cells to perform the global RNA-sequencing analysis (RNA-seq). Analysis of genes expressed differentially were determined by comparing the transcriptomes of SARS-CoV-2-infected cells with 2-D08 treatment with that of non-treated infection group as control. The cut-off of fold change (FC) ratio ($|\log2FC| \geq 1$) and P value ($p$ value < 0.05) were used to identify differentially expressed genes (DEGs). The gene-ontology enrichment analyses illustrated that a number of pathways in SARS-CoV-2 infection were down-regulated in response to 2-D08 treatment (Fig. 7e). The heatmap of genes associated with cytokines and chemokines activity revealed that 2-D08 treatment reduced the cellular immune responses to SARS-CoV-2 infection (Fig. 7f). Genes associated signatures with SARS-CoV-2 infection (such as *IFNB1*, *ISG15*, *IFNL1*, *IFNL2*, *CXCL10*, and *CCR1*) were further identified in IGV genome browser (Fig. 7g). Consistently, GSEA analysis showed enrichment (FDR < 0.01) for signatures associated with ‘viral genome replication’ and ‘response to virus’ (Extended Data Fig. 7a,b). Additional qPCR analysis further confirmed the inhibitory role of 2-D08 and ML-792 in SARS-CoV-2 invasion (Extended Data Fig. 7c,d). To address the functional importance of SUMOylation of ACE2 in SARS-CoV-2 infection, we knocked down the expression of *PIAS4* and found that *PIAS4* depletion suppresses the entry of SARS-CoV-2 (Extended Data Fig. 7e). Additionally, we obtained the converse results in *SENP3* deficient cells (Extended Data Fig. 7f). Taken together, all these results suggested that SUMOylation maintains the stability of ACE2, thereby contributing to the host susceptibility to SARS-CoV-2 infection (Extended Data Fig. 7g).

# Discussion

The recently emerged human pandemic coronavirus SARS-CoV-2, the causative agent of COVID-19, has resulted in substantial morbidity and mortality worldwide[25, 26]. In order to defeat SARS-CoV-2, an urgent demand of unmasking the host–pathogen biology of COVID-19 as this will offer important insights into antiviral treatment. The viral envelope of SARS-CoV-2 is coated by spike protein trimers targets ACE2 receptor, which is the primary viral entry point for coronavirus[27]. ACE2 binding to the SARS-CoV-2 protein spike triggers viral fusion with cell plasma membrane, resulting in viral RNA genome delivery into the host[28]. ACE2 is a carboxypeptidase with several known physiological functions, including regulation of blood pressure, salt and water balance in mammals, amino acid uptake in the small intestine, and glucose homeostasis and pancreatic β-cell function[29]. Whereas, comprehensive understanding of the post-translational modifications of ACE2 and its turnover process, such as in response to viral infection, remains largely unclear. In this study, we investigated the protein interaction and regulation of ACE2

through mass spectrometry analysis, and verified that SUMO pathway is involved in the system-wide identification. We elucidated that ACE2 receptor is a new target for SUMO modification and specific covalent attachment of SUMO3 to ACE2 mediates the ACE2 stabilization. SUMO E3 ligase PIAS4 facilitates the conjugation of SUMO3 to ACE2 at K187, while deSUMOylating enzyme SENP3 removes the attachment of SUMO3 to ACE2. In view of the fact that SUMO modification functions as a positive mediator in the tightly control of ACE2 stability, reversible SUMOylation of ACE2 can be considered as pharmacological targets in antiviral therapy of COVID-19.

Notably, SUMOylation is a post-translational modification regulating numerous cellular processes, including cell cycle progression and DNA damage response[21]. Though the majority of SUMO targets are localized in the nucleus and are thought to undergo rapid cycles of SUMO conjugation and deconjugation[20], our knowledge towards SUMOylation of cytoplasmic proteins is quite limited. Herein, we revealed that SUMO3 modification impedes the K48-linked ubiquitination and autophagic degradation of ACE2. Our results suggested that at least three forms of ACE2 exist: ACE2 SUMOylated at K178, ACE2 modified by K48-linked poly-ubiquitination at K178, and unmodified ACE2. SUMOylation would block the K48-linked ubiquitination of ACE2 at K187. Therefore, the collaborative crosstalk between SUMO and ubiquitin is of great significance for maintaining the protein level of ACE2 via manipulating selective autophagy.

Mounting evidence has supported the critical role of ubiquitination in the recognition of cargo proteins during selective autophagy[15, 30]. However, the substrates and mechanisms of selective autophagy wait to be further explored. We observed the regulatory roles of PIAS4 and SENP3 are abrogated in *TOLLIP* depletion cells and revealed that cargo receptor TOLLIP arrests ACE2 to deliver it to autophagosome for subsequent degradation. TOLLIP has also been shown to facilitate endosomal organization and cargo trafficking, dependent on an association with the ubiquitylated cargo receptor p62 and the ubiquitin E3 ligase RNF26, indicating a potentially important function for TOLLIP in directing ubiquitylation of E3 substrates or their subsequent trafficking[24, 31]. Our data indicate that a TOLLIP-ACE2 interaction is dependent on the TOLLIP CUE domain, but is not perturbed by a defect in the membrane recruitment, and TOLLIP delivers the K48-linked ubiquitylated ACE2 to autophagosomes. Previous evidence has discovered that TOLLIP plays an essential role in the interleukin-1 receptor (IL-1R) and Toll-like receptor (TLR)-mediated innate immune signaling pathways[32]. As a modulator of the immune pathway, TOLLIP indirectly controls the amounts of antimicrobial peptides to prevent infection[33, 34]. In humans, common genetic variation in the TOLLIP gene is concerned to link with susceptibility to multiple intracellular infections[35]. Our findings proved that ubiquitylated ACE2 serves as new substrate of TOLLIP, and TOLLIP influences SARS-CoV-2 infection through selective autophagy in a ubiquitin signal-dependent manner.

Altogether, we demonstrated that dynamic SUMOylation strictly manipulates the protein stability of ACE2 and contributes to the SARS-CoV-2 invasion. SUMOylation inhibitor 2-D08 restrains the cellular entry of SARS-CoV-2 as well as the virus-triggered immune responses of host cells. Our findings uncovered a mechanism underpinning TOLLIP-mediated selective autophagic degradation of ACE2 based on dynamic

changes between SUMOylation and ubiquitination, which affects the entry of SARS-CoV-2 and points out potential pharmacological targets for the therapy of SARS-CoV-2 infection.

# References


1. Gandhi, R.T., Lynch, J.B. & del Rio, C. Mild or moderate Covid-19. *N. Engl. J. Med.* **383**, 1757-1766 (2020).
2. Dhama, K. *et al.* Coronavirus disease 2019-COVID-19. *Clin. Microbiol. Rev.* **33**, 48 (2020).
3. Lv, Z. *et al.* Structural basis for neutralization of SARS-CoV-2 and SARS-CoV by a potent therapeutic antibody. *Science* **369**, 1505-1509 (2020).
4. Li, W.H. *et al.* Angiotensin-converting enzyme 2 is a functional receptor for the SARS coronavirus. *Nature* **426**, 450-454 (2003).
5. Shang, J. *et al.* Cell entry mechanisms of SARS-CoV-2. *Proc. Natl. Acad. Sci. U. S. A.* **117**, 11727-11734 (2020).
6. Hoffmann, M. *et al.* SARS-CoV-2 cell entry depends on ACE2 and TMPRSS2 and is blocked by a clinically proven protease inhibitor. *Cell* **181**, 271-280 (2020).
7. Shang, J. *et al.* Structural basis of receptor recognition by SARS-CoV-2. *Nature* **581**, 221-224 (2020).
8. Monteil, V. *et al.* Inhibition of SARS-CoV-2 infections in engineered human tissues using clinical-grade soluble human ACE2. *Cell* **181**, 905-913 (2020).
9. Tay, M.Z., Poh, C.M., Renia, L., MacAry, P.A. & Ng, L.F.P. The trinity of COVID-19: immunity, inflammation and intervention. *Nat. Rev. Immunol.* **20**, 363-374 (2020).
10. Reynolds, H.R. *et al.* Renin-angiotensin-aldosterone system inhibitors and risk of Covid-19. *N. Engl. J. Med.* **382**, 2441-2448 (2020).
11. Nakatogawa, H. Mechanisms governing autophagosome biogenesis. *Nat. Rev. Mol. Cell Biol.* **21**, 439-458 (2020).
12. Mizushima, N. A brief history of autophagy from cell biology to physiology and disease. *Nat. Cell Biol.* **20**, 521-527 (2018).
13. Gatica, D., Lahiri, V. & Klionsky, D.J. Cargo recognition and degradation by selective autophagy. *Nat. Cell Biol.* **20**, 233-242 (2018).
14. Kirkin, V. & Rogov, V.V. A diversity of selective autophagy receptors determines the specificity of the autophagy pathway. *Mol. Cell* **76**, 268-285 (2019).
15. Johansen, T. & Lamark, T. Selective autophagy: ATG8 family proteins, LIR motifs and cargo receptors. *J. Mol. Biol.* **432**, 80-103 (2020).
16. Jin, S.H. *et al.* Tetherin suppresses type I interferon signaling by targeting MAVS for NDP52-mediated selective autophagic degradation in human cells. *Mol. Cell* **68**, 308-322 (2017).
17. Levy, J.M.M., Towers, C.G. & Thorburn, A. Targeting autophagy in cancer. *Nat. Rev. Cancer* **17**, 528-542 (2017).

18. Hendriks, I.A. & Vertegaal, A.C.O. A comprehensive compilation of SUMO proteomics. *Nat. Rev. Mol. Cell Biol.* **17**, 581-595 (2016).
19. Li, C.Y. *et al.* Quantitative SUMO proteomics identifies PIAS1 substrates involved in cell migration and motility. *Nat. Commun.* **11**, 14 (2020).
20. Seeler, J.S. & Dejean, A. SUMO and the robustness of cancer. *Nat. Rev. Cancer* **17**, 184-197 (2017).
21. Jansen, N.S. & Vertegaal, A.C.O. A chain of events: regulating target proteins by SUMO polymers. *Trends Biochem.Sci.* **46**, 113-123 (2021).
22. Jin, S.H. *et al.* USP19 modulates autophagy and antiviral immune responses by deubiquitinating Beclin-1. *Embo J.* **35**, 866-880 (2016).
23. Lu, K., Psakhye, I. & Jentsch, S. Autophagic clearance of polyQ proteins mediated by ubiquitin-Atg8 adaptors of the conserved CUET protein family. *Cell* **158**, 549-563 (2014).
24. Ryan, T.A. *et al.* Tollip coordinates Parkin-dependent trafficking of mitochondrial-derived vesicles. *Embo J.* **39**, 1-21 (2020).
25. Vindegaard, N. & Benros, M.E. COVID-19 pandemic and mental health consequences: Systematic review of the current evidence. *Brain Behav. Immun.* **89**, 531-542 (2020).
26. Guo, T. *et al.* Cardiovascular implications of fatal outcomes of patients with coronavirus disease 2019 (COVID-19). *JAMA Cardiol.* **5**, 811-818 (2020).
27. Zhang, H.B., Penninger, J.M., Li, Y.M., Zhong, N.S. & Slutsky, A.S. Angiotensin-converting enzyme 2 (ACE2) as a SARS-CoV-2 receptor: molecular mechanisms and potential therapeutic target. *Intensive Care Med.* **46**, 586-590 (2020).
28. Wang, Q.H. *et al.* Structural and functional basis of SARS-CoV-2 entry by using human ACE2. *Cell* **181**, 894-904 (2020).
29. Zheng, Y.Y., Ma, Y.T., Zhang, J.Y. & Xie, X. COVID-19 and the cardiovascular system. *Nat. Rev. Cardiol.* **17**, 259-260 (2020).
30. Khaminets, A., Beh, C. & Dikic, I. Ubiquitin-dependent and independent signals in selective autophagy. *Trends Cell Biol.* **26**, 6-16 (2016).
31. Jongsma, M.L.M. *et al.* An ER-associated pathway defines endosomal architecture for controlled cargo transport. *Cell* **166**, 152-166 (2016).
32. Burns, K. *et al.* Tollip, a new component of the IL-1RI pathway, links IRAK to the IL-1 receptor. *Nat. Cell Biol.* **2**, 346-351 (2000).
33. Akira, S. Toll-like receptor signaling. *J. Biol. Chem.* **278**, 38105-38108 (2003).
34. Shah, J.A. *et al.* Human TOLLIP regulates TLR2 and TLR4 signaling and its polymorphisms are associated with susceptibility to tuberculosis. *J. Immunol.* **189**, 1737-1746 (2012).
35. Huang, C. *et al.* Tollip SNP rs5743899 modulates human airway epithelial responses to rhinovirus infection. *Clinical and Experimental Allergy* **46**, 1549-1563 (2016).
36. Liu, T. *et al.* NOD-like receptor family, pyrin domain containing 3 (NLRP3) contributes to inflammation, pyroptosis, and mucin production in human airway epithelium on rhinovirus infection.

*J. Allergy Clin. Immunol.* **144**, 777-787 (2019).

37. Barry, R. *et al.* SUMO-mediated regulation of NLRP3 modulates inflammasome activity. *Nat. Commun.* **9**, 14 (2018).
38. Wu, Y.X. *et al.* Main protease of SARS-CoV-2 serves as a bifunctional molecule in restricting type I interferon antiviral signaling. *Signal Transduct. Target. Ther.* **5**, 3 (2020).
39. Sun, J. *et al.* Isolation of infectious SARS-CoV-2 from urine of a COVID-19 patient. *Emerg. Microbes Infect.* **9**, 991-993 (2020).
40. Huang, B. *et al.* Mucosal profiling of pediatric-onset colitis and IBD reveals common pathogenics and therapeutic pathways. *Cell* **179**, 1160-1176 (2019).
41. Liao, Y., Smyth, G.K. & Shi, W. featureCounts: an efficient general purpose program for assigning sequence reads to genomic features. *Bioinformatics* **30**, 923-930 (2014).
42. Love, M.I., Huber, W. & Anders, S. Moderated estimation of fold change and dispersion for RNA-seq data with DESeq2. *Genome Biol.* **15**, 1-21 (2014).
43. Yu, G.C., Wang, L.G., Han, Y.Y. & He, Q.Y. clusterProfiler: an R package for comparing biological themes among gene clusters. *Omics* **16**, 284-287 (2012).
44. Ramirez, F. *et al.* deepTools2: a next generation web server for deep-sequencing data analysis. *Nucleic Acids Res.* **44**, 160-165 (2016).

# Methods

**Cell lines and culture conditions.** HEK293T (human embryonic kidney 293T), HeLa, and A549 cells were cultured in DMEM medium (Gibco) with 10% (vol/vol) fetal bovine serum (Gibco) and 1% glutamine (Gibco). Calu-3 cells were cultured in MEM (Gibco) with 1% NEAA (Gibco), 1% sodium pyruvate (Gibco) and 10% (vol/vol) fetal bovine serum (Gibco). Primary nasal epithelial cells (hNEPCs) were isolated from fresh nasal specimens by means of enzymatic digestion with Dispase II (Sigma) at 48 °C overnight. Biopsy specimens of nasal mucosa were obtained from patients with chronic rhinosinusitis (CRS) who underwent functional endoscopic surgery at the First Affiliated Hospital, Sun Yat-sen University, Guangzhou, China. None of the patients had other systemic diseases and did not receive glucocorticoids, antibiotics, or both within 3 months before the study. Approval to conduct this study was obtained from the Institutional Review Board of the First Affiliated Hospital, Sun Yat-sen University. All patients provided written informed consent. A modified culture method based on the previous described[36]. To induce starvation, cells were washed with phosphate-buffered saline (PBS) and incubated in EBSS (Gibco). All cells were incubated at 37 °C incubator with 5% $CO_2$.

**Antibodies and reagents.** Horseradish peroxidase anti-Flag (M2; A8592) and anti-β-actin (A1978) were purchased from Sigma. Horseradish peroxidase anti-hemagglutinin (HA; 12013819001) and anti-c-myc (Myc; 11814150001) were purchased from Roche Applied Science. Anti-ACE2 (21115-1-AP), anti-PIAS4 (14242-1-AP), anti-Beclin-1 (11306-1-AP), anti-ATG5 (10181-2-AP), anti-p62/SQSTM1 (18420-1-AP) and anti-TOLLIP (11315-1-AP) were acquired from Proteintech. K48-linkage specific polyubiquitin antibody

(4289) and anti-ACE2 (4355) were purchased from Cell Signaling Technology. Anti-SENP3 (sc-133149), anti-SUMO1 (sc-5308), and anti-SUMO2/3/4 (sc-393144) were from Santa Cruz Biotechnology. Anti-CoV2-N (40588-T62) was acquired from Sino Biological. ML-792 (HY-108702) and 2-D08 (HY-114166) were from MedChemExpress (MCE). MG132 (C-2211), 3-methyladenine (M9281), bafilomycin A1 (H2714), and *N*-Ethylmaleimide (NEM) (E3876) were purchased from Sigma.

**Plasmids and siRNA Transfection.** Constructs coding for ACE2 were cloned in the pcDNA3.1 vector for transient expression and into the FG-EH-DEST (provided by Xiaofeng Qin laboratory) for retroviral expression. HEK293T transfection was performed using Lipofectamine 2000 (Invitrogen) according to procedures recommended by the manufacturer. Chemically synthesized 21-nucleotide siRNA duplexes were obtained from Sangon Biotech and transfected using Lipofectamine RNAiMAX (Invitrogen) according to the manufacturer's instructions. siRNA sequences were:

*Scramble* (*Scr*) siRNA: 5'-GUGAGCGUCUAUAUACCAUTT-3';

*PIAS4* siRNA #1: 5'-GGAGUAAGAGUGGACUGAATT-3';

*PIAS4* siRNA #2: 5'-GCUCUACGGAAAGUACUUATT-3';

*TOLLIP* siRNA #1: 5'-CACACAAUGGCGCCAAGAAUCTT-3';

*TOLLIP* siRNA #2: 5'-CGACUGAACAUCACGGUGGUATT-3';

*SENP3* siRNA #1: 5'-ACGUGGACAUCUUCAAUAATT-3';

*SENP3* siRNA #2: 5'-CAAUAAGGAGCUACUGCUATT-3'.

**Generation of stable expression cell lines.** For ACE2 ectopic expression, lentiviral particles were produced by transfecting HEK293T cells with FG-EH-DEST-ACE2-Puro, VSGV and Δ8.9. The medium was changed the following day and the viral containing supernatant was collected 48 hr after transfection, filtered through a 0.45 mm filter. A549 cells were infected by incubation with lentivirus-containing supernatant for 48 hr together with Polybrene (8 μg $ml^{-1}$). Transduced cells were purified by puromycin selection. For *SENP* KO cells, target sequences were cloned into pLentiCRISPRv2 by cutted with *Bsm*BI. The target sequences used were as follows:

SENP1 target: 5'-TCGGTCCAAATGTCCTTGCC-3';

SENP2 target: 5'-GCACCGACCGGTCGCAGAAA-3';

SENP3 target: 5'-GTGGCGTCGCACCCCCTTGC-3';

SENP5 target: 5'-GGACCATCAAGAGACCCGTA-3';

SENP6 target: 5'-GTAAGGTTAAGTCGGCTCCA-3'

SENP7 target: 5'-GAGTCTAGTATAAGAATACA-3';

SENP8 target: 5'-GGTCCATCTTGTACTGACGA-3'.

**Quantitative RT-PCR.** Total RNA was extracted from cells using the TRIzol reagent (Invitrogen) according to the manufacturer's instructions. For RT-PCR analysis, cDNA was generated with HiScript® II Q RT SuperMix for qPCR (+gDNA wiper) (Vazyme, R223-01) and was analyzed by quantitative real-time PCR using the 2 × RealStar Green Power Mixture (GenStar). All data were normalized to *RPL13A* expression. The primer pair sequences were as follows: *RPL13A* Fwd, 5'-GCCATCGTGGCTAAACAGGTA-3' and *RPL13A* Rev, 5'-GTTGGTGTTCATCCGCTTGC-3'; *PIAS4* Fwd, 5'- TCAGATGCTCCTGGGTTTCGTG-3' and *PIAS4* Rev, 5'- TTCTTCTTGGCGTAGCGGGTC-3'; *ACE2* Fwd, 5'- CTTTCCGTCTGAATGACAACA-3' and *ACE2* Rev, 5'- CACTATCACTCCCATCACAACTC-3'; *SARS-CoV-2-NSP10* Fwd, 5'-CCCTGTGGGTTTTACACTTAA-3' and *SARS-CoV-2-NSP10* Rev, 5'-ACGATTGTGCATCAGCTGA-3'; *SARS-CoV-2-N* Fwd, 5'-GGGGAACTTCTCCTGCTAGAAT-3' and *SARS-CoV-2-N* Rev, 5'-CAGACATTTTGCTCTCAAGCTG-3'; *TNFA* Fwd, 5'-CCTCTCTCTAATCAGCCCTCTG-3' and *TNFA* Rev, 5'-GAGGACCTGGGAGTAGATGAG-3'; *IFNL1* Fwd, 5'-GTGACTTTGGTGCTAGGCTTG-3' and *IFNL1* Rev, 5'-GCCTCAGGTCCCAATTCCC-3'; *CXCL10* Fwd, 5'-GTGGCATTCAAGGAGTAGCTC-3' and *CXCL10* Rev, 5'-GCCTTCGATTCTTGGATTCAG-3'.

**Immunoprecipitation and immunoblot analysis.** For immunoprecipitation, whole-cell extracts were prepared after transfection or stimulation with appropriate ligands, followed by incubation overnight with the appropriate antibodies plus Protein A/G beads (Pierce). For immunoprecipitation with anti-Flag, α-FLAG M2 beads (Sigma) were used. Beads were then washed five times with low-salt lysis buffer (50 mM HEPES, 150 mM NaCl, 1mM EDTA, 10% glycerol, 1.5 mM $MgCl_2$, and 1% Triton X-100), and immunoprecipitates were eluted with 2 × SDS Loading Buffer and resolved by SDS-PAGE. Proteins were transferred to PVDF membranes (Bio-Rad) and further incubated with the appropriate antibodies. Immobilon Western Chemiluminescent HRP Substrate (Millipore) was used for protein detection.

**Mass spectrometry analysis.** Total lysates were prepared from 293T cells transfected with Flag-ACE2 and followed by immunoprecipitation with α-FLAG M2 beads. Immunoprecipitated proteins were separated by SDS-PAGE, and then stained with Coomassie Blue. The entire lane was excised, digested with trypsin and analyzed with LC-MS/MS. LC-MS/MS identification of peptide mixtures was performed at Applied Protein Technology (aptbiotech, Inc. Shanghai, China). Briefly, peptides were chromatographed through the Easy-nLC 1000 system (Thermo Fisher, California, USA). Peptide samples were loaded by Thermo Scientific Acclaim PepMap100 (100 μm*2 cm, nanoViper C18) and separated by Thermo scientific EASY column (10 cm, ID75 μm, 3 μm, C18-A2) at 300 nL $min^{-1}$ for 60 min using a three-step acetonitrile (0.1% formic acid in 84% acetonitrile) gradient: 0–35% over the first 50 min and 35–100% for 50–55 min and 100% for 55–60 min. The tandem mass spectrometry was performed by Q Exactive mass spectrometer (Thermo Fisher, California, USA). The MS1 survey scan (300–1800 *m/z*) was at a resolution of 70,000 at 200 *m/z* with automatic gain control (AGC) target of 1e6 and a maximum injection time of 50 ms. Dynamic exclusion was 60.0 s. Each full scan takes 20 MS2 scans. MS2 activation type was HCD model. Isolation window was 2 *m/z*. MS2 scan was at a resolution of 17,500 at 200 *m/z* with normalized collision energy

30 eV. Underfill was 0.1%. RAW files generated by spectrometer was subjected to Biopharma Finder1.0 software for protein identification.

**SUMOylation assay and prediction of SUMOylation sites.** For SUMOylation assays, $2 \times 10^6$ 293T cells were plated in 10 cm dishes and transfected with a total of 7.5 µg of DNA the following day. 48 hr post-transfection cells were lysed in low-salt lysis buffer supplemented with deSUMOylation inhibitor NEM (20 mM) and complete protease inhibitors. Cell lysates were sonicated for 20 s then clarified at 4 °C at 12,000 g for 5 min. 20 µl of α-FLAG M2 beads was rotated with cleared protein lysates at 4°C for overnight. Furthermore, 4 × washes in low-salt lysis buffer, supplemented with NEM (20 mM) and complete protease inhibitors, were performed, and samples eluted by boiling in 15 µl 2 × SDS loading dye. For the prediction of putative SUMOylation sites in ACE2, GPS-SUMO, SUMOplot analysis (Abgent) software, JASSA and Ron Hay's SUMO consensus motif search tool were used as previously described[37].

**Fluorescence microscopy.** Cells were cultured on Glass Bottom culture dishes (Nest Scientific) and directly observed as previously described[16]. For examination by immunofluorescence microscopy, cells were fixed with 4% paraformaldehyde for 10 min, and then permeabilized in methyl alcohol for 30 min at −20 °C. After washing with PBS for 3 times, cells were blocked in 5% goat serum for 1 hr, and then incubated with primary antibodies diluted in 5% goat serum overnight. The cells were washed and followed by a fluorescently labeled secondary antibody (CF488A rabbit anti-HA IgG, Biotium; Rabbit IgG (H+L) highly cross-adsorbed secondary antibody, Alexa Fluor 488, Invitrogen; Goat anti-mouse IgG (H+L) highly cross-adsorbed secondary antibody, Alexa Fluor 488, Invitrogen; Goat anti-mouse IgG (H+L) highly cross-adsorbed secondary antibody, Alexa Fluor 568, Invitrogen; Goat anti-rabbit IgG (H+L) cross-adsorbed secondary antibody, Alexa Fluor 568, Invitrogen; Goat anti-mouse IgG (H+L) cross-adsorbed secondary antibody, Alexa Fluor 633, Invitrogen). Confocal images were examined using a microscope (TCS SP8 STED 3X; Leica) equipped with 100 × 1.40 NA oil objectives. The images were processed for gamma adjustments using Leica AS Lite or ImageJ software (National Institutes of Health). The data plotted on the line intensity plots were produced by using the Plot Profile function of Image J on a single plane z-stack of confocal microscopy pictures.

**Virus infection.** Cells were either mock-infected or infected with SARS-CoV-2 (Accession number: MT123290), as previously described[38, 39]. Virus was allowed to adsorb at 37 °C for 1 hr with gentle rocking every 15 min before incubation at 37 °C for indicated time points. Cells were infected at different MOI and time points as indicated.

**SARS-CoV-2 S pseudotyped virus.** Pseudotyped particles were obtained from package of pHIV-Luciferase, psPAX2, and SARS-CoV-2 S protein expressing pcDNA3.1 vector (all these plasmids are gifts from Yi-Ping Li laboratory). The pseudovirions contain SARS-CoV-2 spike protein and the firefly luciferase gene. Therefore, the spike-mediated cell entry can be measured via luciferase reporter activity.

**Immunofluorescence staining.** Paraffin-embedded sections of lung biopsies were processed as reported previously[40]. Briefly, sections were deparaffinized, incubated with blocking buffer (PBS with 5% normal

donkey or goat serum and 0.3% Triton X-100) at room temperature for 1 hr, and stained with primary antibodies overnight in a wet chamber at 4 °C in the dark. Sections were then washed with PBS, incubated with secondary antibodies (Goat anti-rabbit IgG (H+L) highly cross-adsorbed secondary antibody, Alexa Fluor 488, Invitrogen and goat anti-mouse IgG (H+L) cross-adsorbed secondary antibody, Alexa Fluor 594, Invitrogen) for 1 hr at room temperature in the dark, and mounted with DAPI for nuclear staining. Immunofluorescent images were acquired with a Nikon Eclipse Ni-E microscope using a × 40 objective. Post-acquisition processing (brightness, opacity, contrast, and color balance) was applied to the entire image and accurately reflected the results of the original image. The protein expression levels were quantified in square micrometers by using ImageJ software.

**RNA-seq analysis.** Total RNA was isolated from cells using TRIzol reagent (Invitrogen), and sequencing was performed by Sangon Biotech. Sample quality was assessed using a Bioanalyzer (Agilent 2100 Bioanalyzer). RNA-seq libraries of polyadenylated RNA were prepared using mRNA-seq V2 Library Prep Kit and sequenced on MGISEQ-2000 platform. All clean data were mapped to the human genome GRCh38 using HISAT2 v2.1.0 with default parameters. Bam files were sorted by Samtools 1.9. Reads counts were summarized using the featureCounts program as part of the Subread package release 2.0.0 (http://subread.sourceforge.net/)[41]. To identify differentially expressed genes (DEGs) between groups, DESeq2 was used to normalize reads counts and $p$ value < 0.05 and absolute logged fold-change ≥ 1 were determined as DEGs73 using Bioconductor clusterProfiler package v3.14.3 for the functional enrichment of DEGs[42, 43]. RNA-seq sequence density profiles were normalized using bamCoverage and visualized in IGV genome browser[44].

**Statistical analysis.** Data from three or more experiments were displayed as mean ± SEM unless otherwise indicated, and data of immunofluorescent staining experiments are represented as mean ± SD of indicated image numbers. Student's *t*-test was used for all statistical analyses with the GraphPad Prism 8 software. Differences between two groups were considered significant when $P$ value was less than 0.05.

# Declarations

### Reporting Summary

Further information on research design is available in the Nature Research Reporting Summary linked to this article.

### Data availability

The data that support the findings of this study are available from the corresponding author upon reasonable request. Source data are provided with this paper.

### Acknowledgments

This work was supported by the National Key R&D Program of China (2020YFA0908700 and 2020YFC0842400), National Natural Science Foundation of China (31970700, 92042303 and 31870862), and Guangdong Basic and Applied Basic Research Foundation (2020B1515120090).

### Author contributions

J.C. and S.J. conceived the project and designed the experiments. S.J. and X.H. performed the experiments. L.M., M.L., S.C., L.W., Z.Z., Y.W., J.Z., K.P., Y.Z. and Z.S. provided technical help. S.J. and L.M. analyzed the data. J.C. provided resources, and directed the research. S.J. and J.C. wrote the manuscript. All authors read and approved the final manuscript.

### Competing interests

The authors declare no competing interests.

## Figures

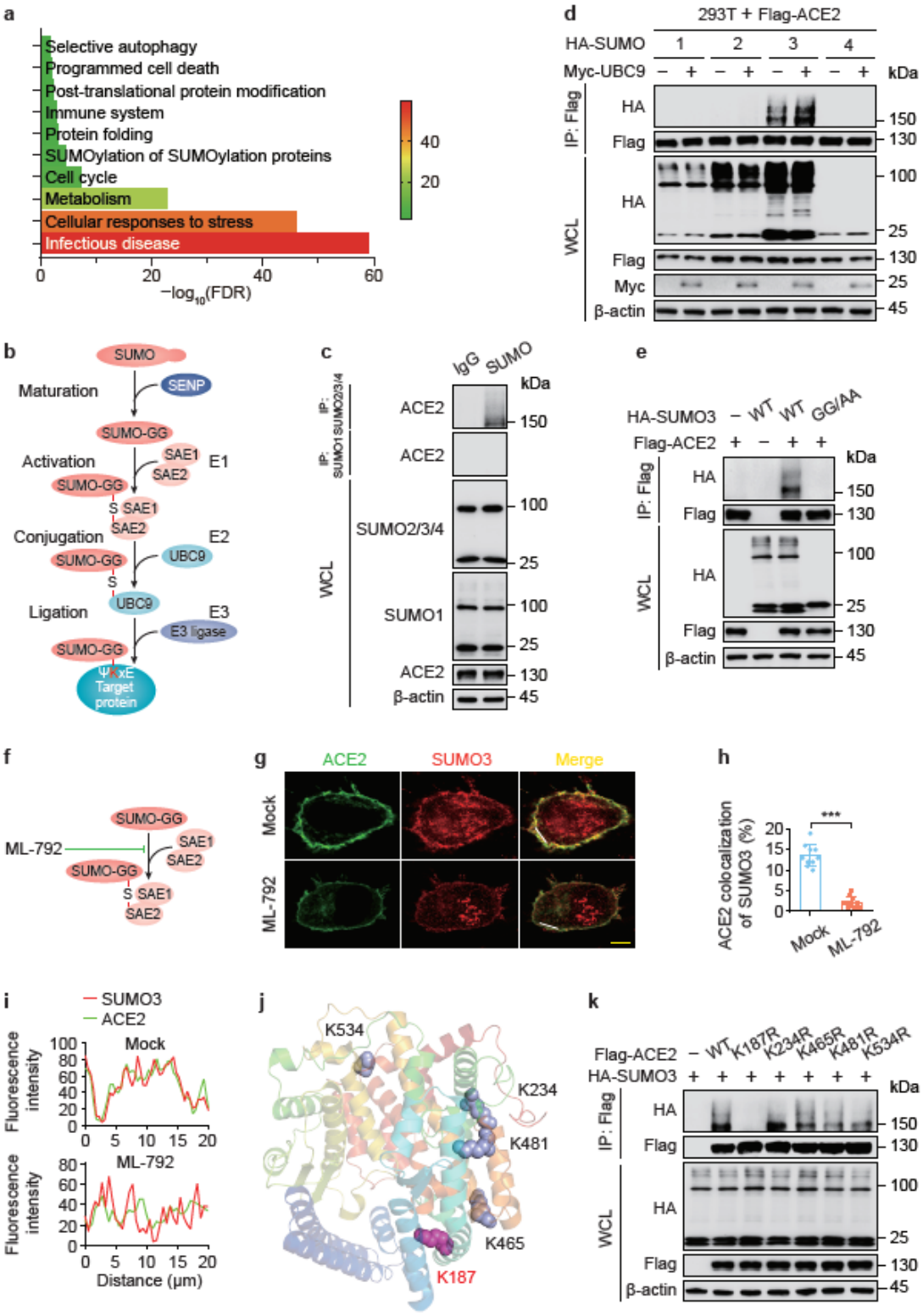


## Figure 1

ACE2 receptor is specifically conjugated with SUMO3. a, Gene Ontology (GO) analysis of the proteome after purified with ACE2 receptor as bait. b, Schematic diagram of the conjugation of small ubiquitin-like modifier (SUMO) with substrates. c, Extracts of Calu-3 cells were subjected to immunoprecipitation with anti-SUMO and immunoblot analysis with indicated antibodies (shown on the left). d, Lysates of 293T cells transfected with plasmids expressing Flag-ACE2 and HA-tagged SUMO, together with the empty

vector or expression vector of Myc-UBC9 were immunoprecipitated with anti-Flag and immunoblotted with anti-HA. e, Lysates of 293T cells transfected with plasmids expressing Flag-ACE2 and HA-SUMO3 and its indicated mutants were immunoprecipitated with anti-Flag and immunoblotted with anti-HA. f, Illustration of the inhibitory site of ML-792. g, Confocal microscopy of HeLa cells transfected with Flag-ACE2, followed by labeling of ACE2 (green) and SUMO3 (red) with specific antibodies. Scale bar, 20 μm. h, Quantitative analysis of the similar samples as (g). i, Histogram shows the fluorescence intensity of ACE2 and SUMO3 along the white segment in the merged fluorescence panel of (g). j, Structure of human ACE2 depicting the identified SUMO motifs. The predicted lysines shown in (i) are highlighted as purple. The structural information of ACE2 was downloaded from Protein Data Bank (ID: 1R42). k, 293T cells were transfected with plasmids encoding HA-SUMO3 and wild-type (WT) Flag-ACE2 or its indicated mutants, followed by immunoprecipitation with anti-Flag beads and immunoblot analysis with anti-HA. Data in (h) are expressed as means ± SD of 10 cells. ***$p < 0.001$. (two-tailed Student's t-test). For data in (c-e, k), similar results were obtained by three independent biological experiments.

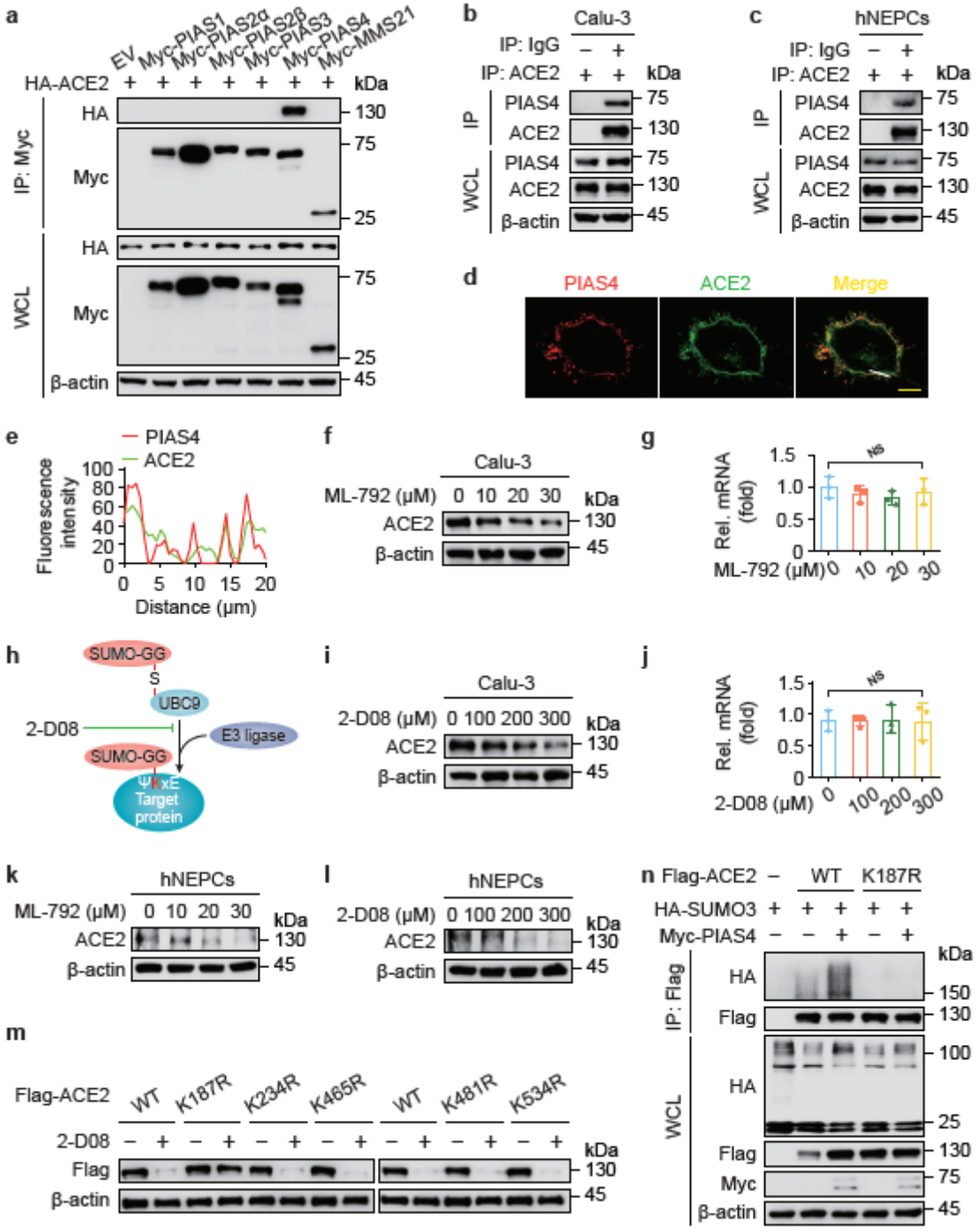


## Figure 2

PIAS4 targets ACE2 for SUMOylation and stabilization. a, 293T cells were transfected with vectors encoding HA-ACE2 and indicated Myc-tagged SUMO E3 ligases, followed by immunoprecipitation with anti-Myc beads and immunoblot analysis with anti-HA. b-c, Extracts of Calu-3 cells (b) and hNEPCs (c) were subjected to immunoprecipitation with anti-ACE2 and immunoblot analysis with indicated antibodies (shown on the left). d, Confocal microscopy of HeLa cells transfected with Flag-ACE2, followed by labeling of ACE2 (green) and PIAS4 (red) with specific antibodies. Scale bar, 20 μm. e, Histogram shows the fluorescence intensity of ACE2 and PIAS4 along the white segment in the merged fluorescence panel of (d). f, Calu-3 cells were treated with indicated concentration of ML-792 for 24 hr,

and the proteins were harvested for immunoblot analysis. g, ACE2 mRNA levels of the same sample (f) were detected by real-time PCR. h, Illustration of the inhibitory site of 2-D08. i, Calu-3 cells were treated with indicated concentration of 2-D08 for 24 hr, and the proteins were harvested for immunoblot analysis. j, ACE2 mRNA levels of the same sample (i) were detected by real-time PCR. k-l, hNEPCs were treated with indicated concentrations of ML-792 (k) or 2-D08 (l) for 24 hr, and the proteins were harvested for immunoblot analysis. m, 293T cells transfected with plasmids expressing wild-type (WT) Flag-ACE2 or its indicated mutants were treated with 2-D08 (200 μM) for 24 hr. Different amounts of plasmids for WT and various mutants of Flag-ACE2 were transfected into cells for equal expression. The lysates were subjected to immunoblot analysis. n, Lysates of 293T cells transfected with plasmids encoding HA-SUMO3 and Flag-ACE2 or its K187R mutant along with vector expressing Myc-PIAS4 were immunoprecipitated with anti-Flag and immunoblotted with anti-HA. Data in (g) and (j) are expressed as means ± SEM of three independent experiments. NS, not significant. (two-tailed Student's t-test). For data in (a-f, i, k-n), similar results were obtained by three independent biological experiments.

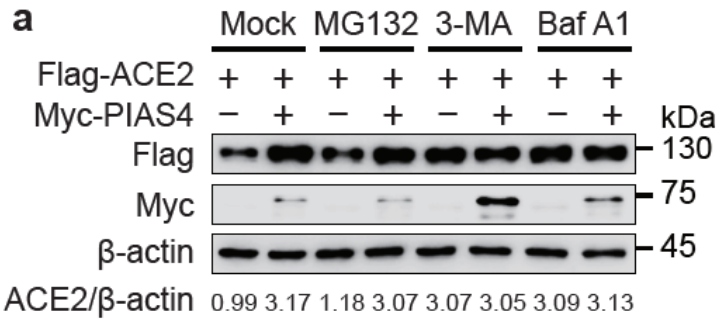


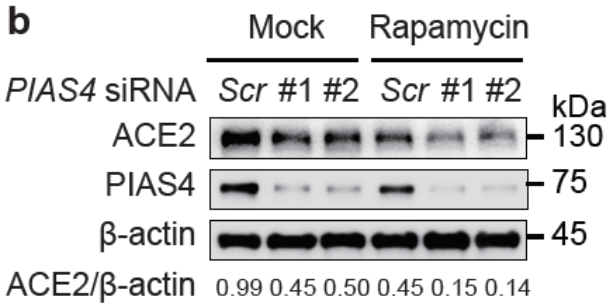


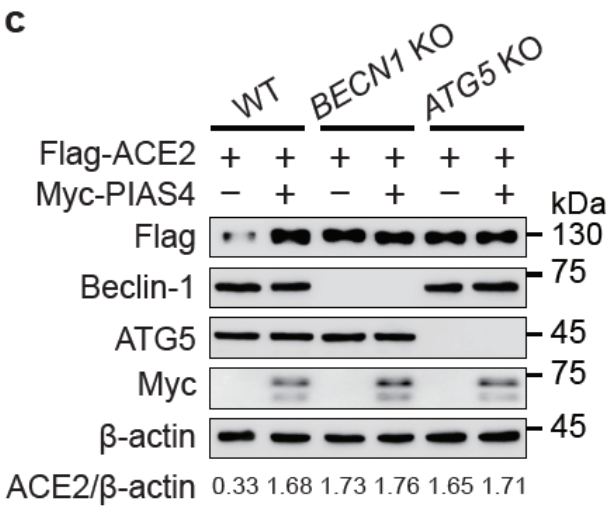


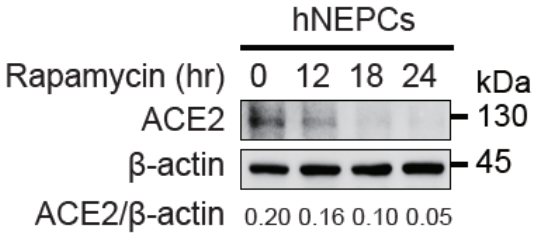


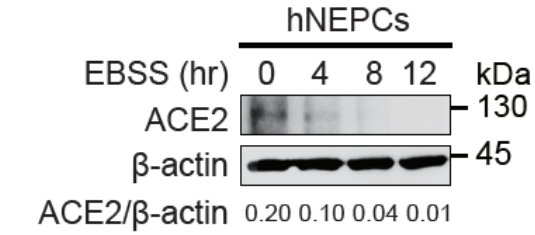


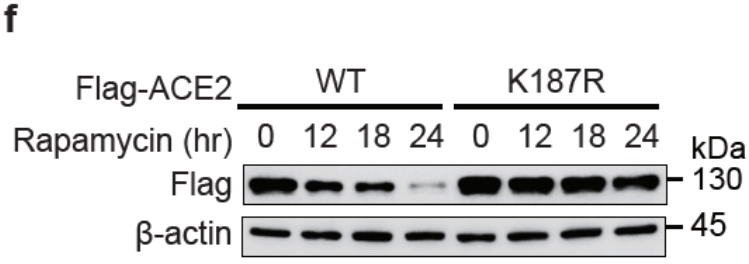


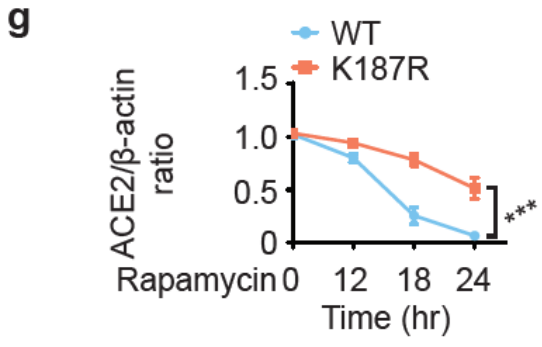

## Figure 3

PIAS4 attenuates the autophagic degradation of ACE2. a, 293T cells were transfected with plasmid encoding Flag-ACE2 together with Myc-PIAS4 vector treated with MG132 (10 μM), 3-methyladenine (3-MA) (10 mM), or bafilomycin A1 (Baf A1) (0.2 μM) for 6 hr. The cell lysates were analyzed by immunoblot. b, Lysates of Calu-3 cells transfected with scramble or PIAS4-specific siRNA, followed by rapamycin (250 nM) treatment for 24 hr, were harvested for immunoblot analysis. c, Wild-type (WT), BECN1 and ATG5 knockout (KO) 293T cells were transfected with plasmids encoding Flag-ACE2 and Myc-PIAS4, the lysates were analyzed with indicated antibodies. d-e, hNEPCs were treated with rapamycin (250 nM) (d) or EBSS (e) for treatment with indicated time points, and the proteins were harvested for immunoblot analysis. f, 293T cells were transfected with Flag-ACE2 (WT or K187R) and treated with rapamycin (250 nM) for indicated time points. The protein levels of Flag-ACE2 were analyzed by immunoblot. g, Quantification of the protein levels of WT and K187R Flag-ACE2 in (f). Data in (g) are expressed as means ± SEM of three independent experiments. ***$p < 0.001$; NS, not significant. (two-tailed Student's t-test). For data in (a-f), similar results were obtained by three independent biological experiments.

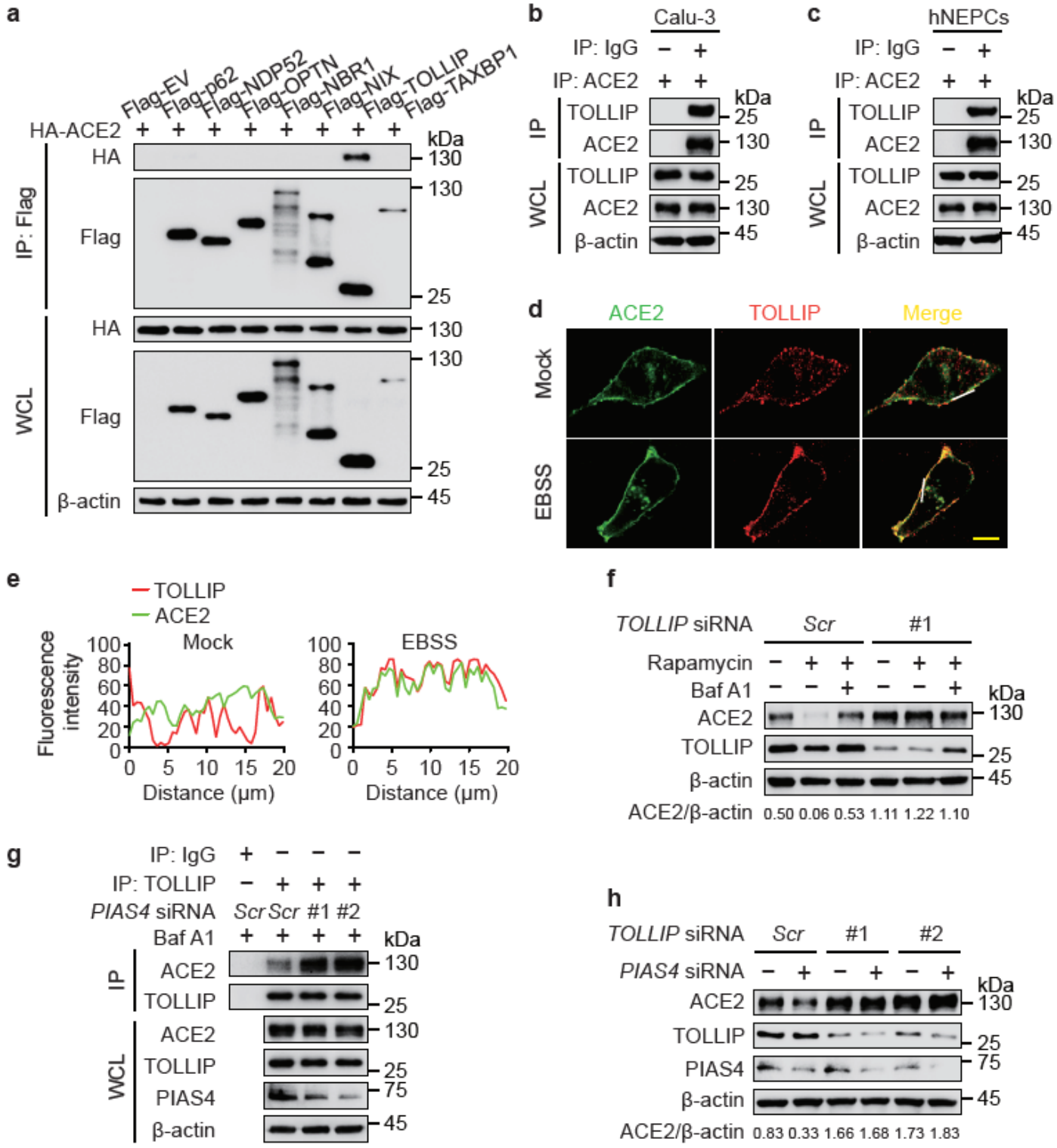


## Figure 4

PIAS4 disrupts the recognition of ACE2 by cargo receptor TOLLIP. a, 293T cells were transfected with vectors encoding HA-ACE2 and indicated Flag-tagged cargo receptors, followed by immunoprecipitation with anti-Flag beads and immunoblot analysis with anti-HA. b-c, Extracts of Calu-3 cells (b) and hNEPCs (c) were subjected to immunoprecipitation with anti-ACE2 and immunoblot analysis with indicated antibodies (shown on the left). d, Confocal microscopy of HeLa cells transfected with Flag-ACE2,

followed by labeling of ACE2 (green) and TOLLIP (red) with specific antibodies. Scale bar, 20 μm. e, Histogram shows the fluorescence intensity of ACE2 and TOLLIP along the white segment in the merged fluorescence panel of (d). f, Lysates of Calu-3 cells transfected with scramble or TOLLIP-specific siRNA, followed by rapamycin (250 nM) treatment for 24 hr together with or without Baf A1 (0.2 μM), were harvested for immunoblot analysis. g, Lysates of Calu-3 cells transfected with PIAS4-specific or scramble siRNA, followed by Baf A1 (0.2 μM) treatment, were subjected to immunoprecipitation with anti-ACE2 and immunoblot analysis with indicated antibodies. h, Calu-3 cells transfected with scramble or TOLLIP-specific siRNA for 8 hr were then transfected with PIAS4-specific siRNA. The protein expression levels of ACE2 were detected by immunoblot. For data in (a-h), similar results were obtained by three independent biological experiments.

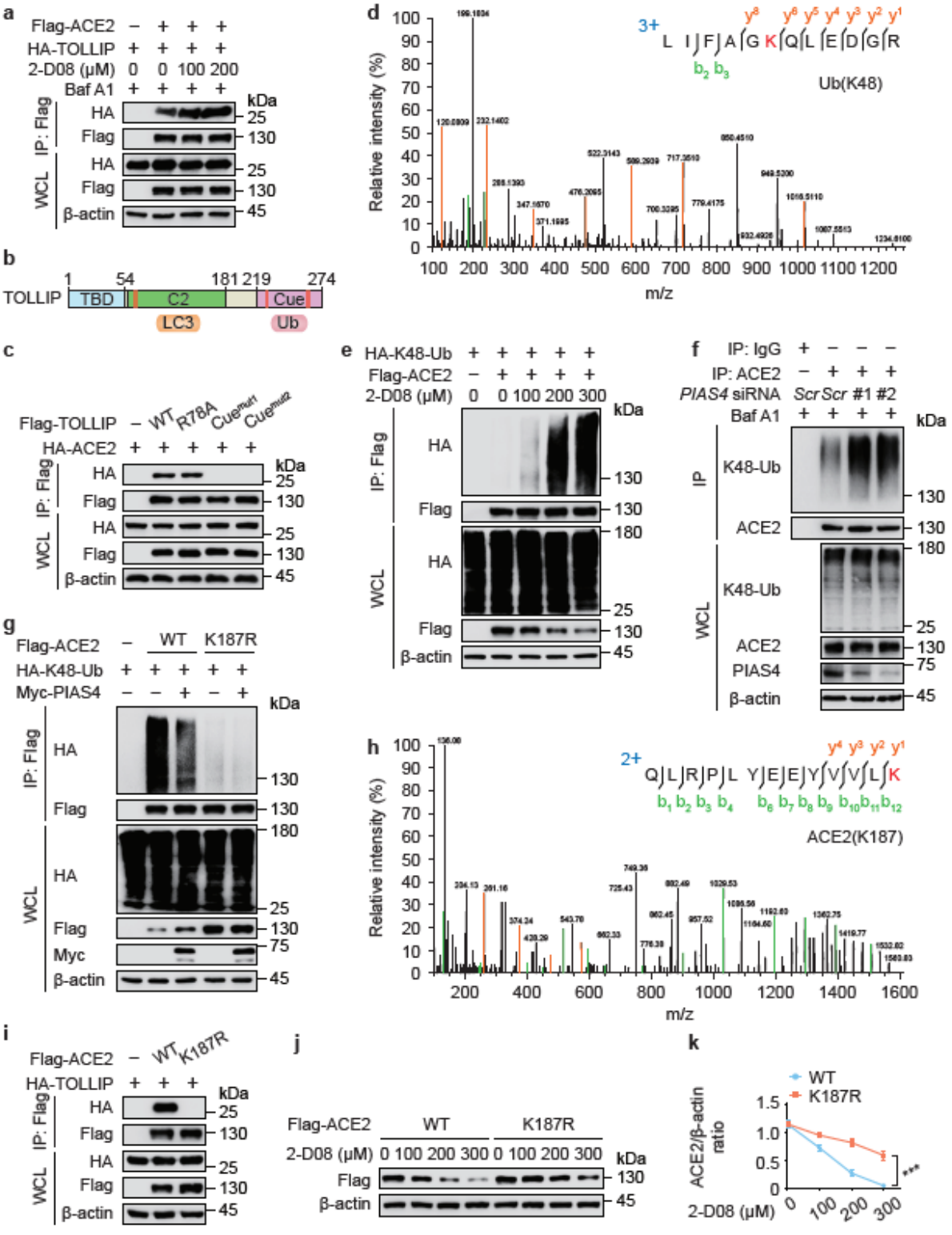


## Figure 5

SUMOylation dampens the K48-linked ubiquitination of ACE2. a, 293T cells were transfected with plasmids encoding Flag-ACE2 and HA-TOLLIP, and treated with indicated concentrations of 2-D08 for 24 hr. The cells cultured with Baf A1 (0.2 μM) for 6 hr were immunoprecipitated with anti-Flag and immunoblotted with anti-HA. b, Domain organization of TOLLIP protein. c, Coimmunoprecipitation and immunoblot analysis of 293T cells transfected with mutants of TOLLIP plasmids along with vector

encoding HA-ACE2. d, Mass-spectrometry analysis of a K48-linked ubiquitin peptide of purified ACE2. e, 293T cells transfected with plasmids expressing Flag-ACE2 and HA-tagged ubiquitin K48 mutant were treated with indicated concentration of 2-D08 for 24 hr. The lysates were subjected to immunoprecipitation and immunoblot analysis. f, Calu-3 cells were transfected with scrambled or PIAS4-specific siRNA. The protein extracts harvested after Baf A1 (0.2 μM) treatment for 6 hr, were immunoprecipitated using anti-ACE2 antibody or with IgG as a negative control and analyzed by immunoblot using K48-linkage specific polyubiquitin antibody and anti-ACE2 antibody. g, Immunoprecipitation and immunoblot analysis of 293T cells transfected with vectors expressing Flag-ACE2 (WT or K187R) and HA-K48-linked ubiquitin in the presence of Myc-PIAS4. h, Mass-spectrometry analysis identified a ubiquitination site on ACE2 at K187. i, 293T cells were transfected with plasmids encoding HA-TOLLIP and wild-type (WT) Flag-ACE2 or its K187R mutant, followed by immunoprecipitation with anti-Flag beads and immunoblot analysis with anti-HA. j, 293T cells were transfected with WT Flag-ACE2 or its K187R mutant and treated with 2-D08 for indicated concentrations. The protein levels of Flag-ACE2 were analyzed by immunoblot. k, Quantification of the protein levels of WT and K187R Flag-ACE2. Data in (k) are expressed as means ± SEM of three independent experiments. ***$p < 0.001$. (two-tailed Student's t-test). For data in (a, c, e-g, i and j), similar results were obtained by three independent biological experiments.

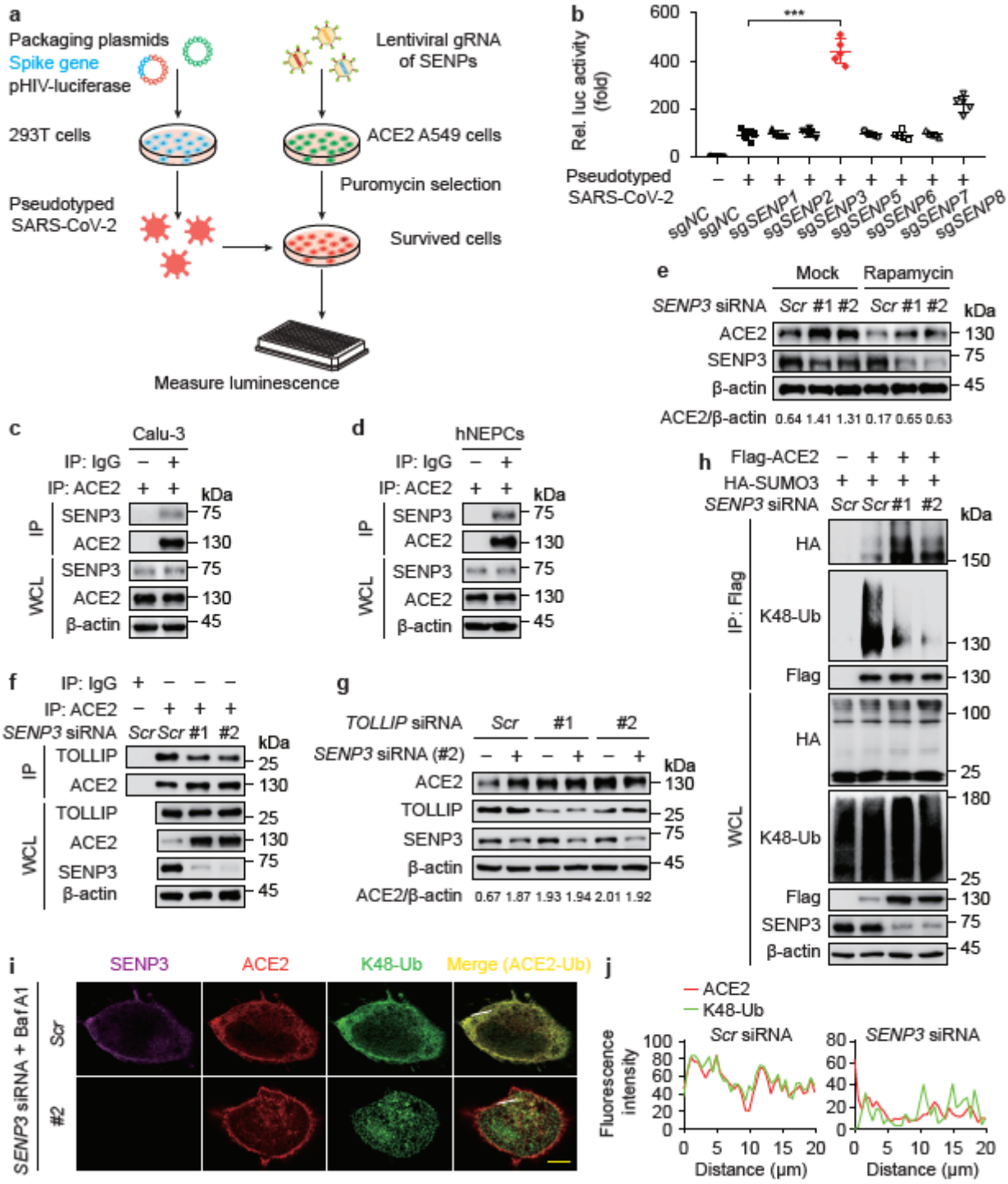


## Figure 6

SENP3 deSUMOylates ACE2 to prompt its K48-liked ubiquitination and autophagic degradation. a, Overview of the screening for functional deSUMOylating enzymes in human ACE2-expressing A549 cells with the infection of SARS-CoV-2 S pseudotyped virus. b, Luciferase activity in control and deSUMOylating enzyme depletion human ACE2-expressing A549 cells infected with SARS-CoV-2 S pseudotyped virus. c-d, Extracts of Calu-3 cells (c) and hNEPCs (d) were subjected to immunoprecipitation with anti-ACE2 and immunoblot analysis with indicated antibodies. e, Lysates of

Calu-3 cells transfected with scramble or SENP3-specific siRNAs treated with rapamycin (250 nM) for 24 hr. The proteins were harvested for immunoblot analysis. f, Protein extracts of Calu-3 cells transfected with scrambled or SENP3 siRNA were immunoprecipitated using anti-ACE2 antibody or with IgG as a negative control and analyzed by immunoblot using indicated antibodies. g, Calu-3 cells transfected with scramble or TOLLIP-specific siRNA for 8 hr, followed by SENP3-specific siRNA transfection were subjected to immunoblot analysis. h, 293T cells transfected with scramble or SENP3-specific siRNAs were then transfected with plasmids encoding Flag-ACE2 and HA-SUMO3. The proteins were harvested for immunoprecipitation and immunoblot analysis. i, Confocal microscopy of HeLa cells transfected with scramble or SENP3-specific siRNA and then transfected with Flag-ACE2 and HA-K48-linked ubiquitin plasmids, followed by labeling of SENP3 (purple), ACE2 (red) and HA-K48-linked ubiquitin (green) with specific antibodies. Scale bar, 20 μm. j, Histogram shows the fluorescence intensity of ACE2 and HA-K48-linked ubiquitin along the white segment in the merged fluorescence panel of (i). Data in (b) are expressed as means ± SEM of three independent experiments. For data in (c-j), similar results were obtained by three independent biological experiments.

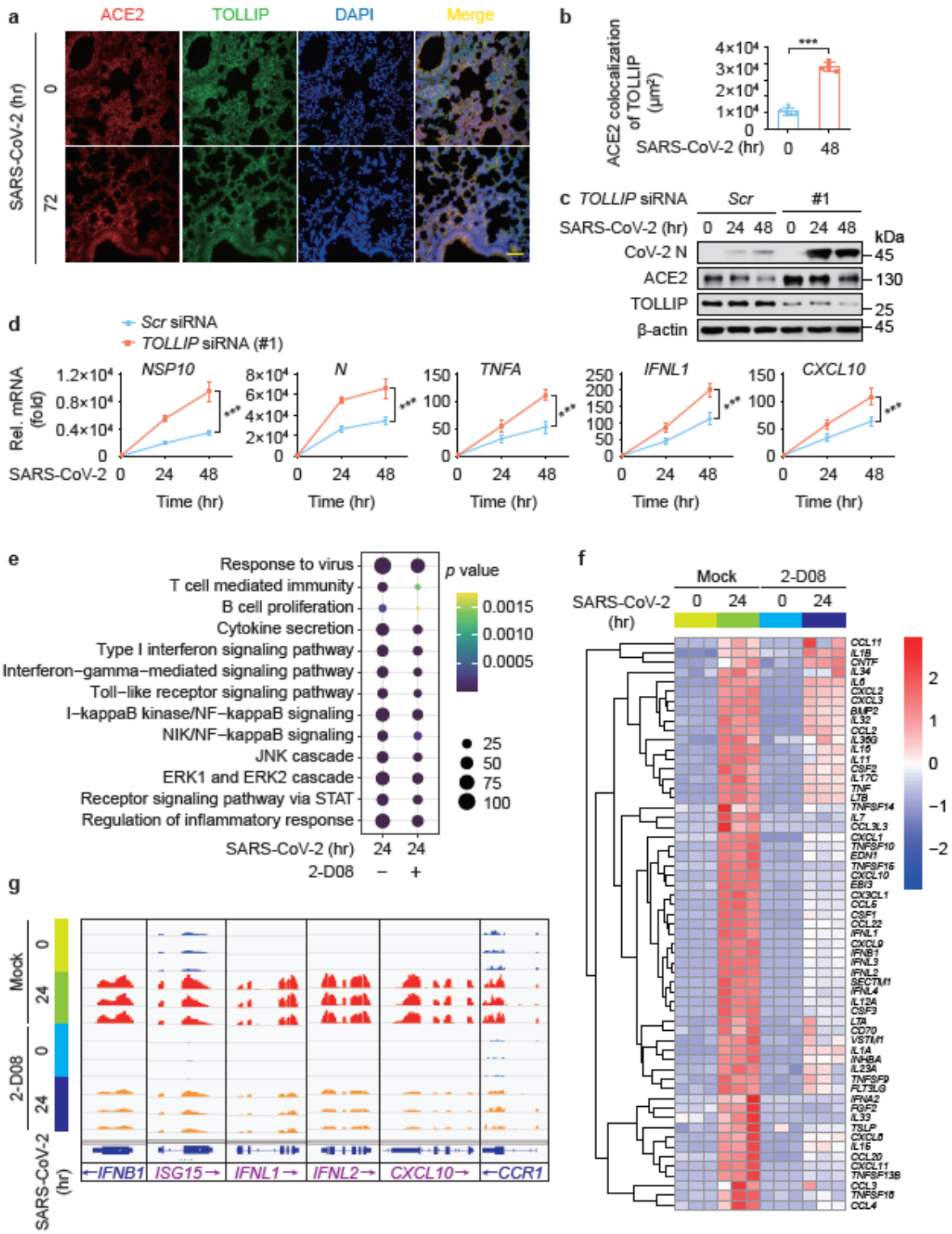


## Figure 7

Manipulation ACE2 SUMOylation modulates the SARS-CoV-2 entry and the subsequent immune responses. a, Representative ACE2 (red) and TOLLIP (green) immunofluorescent staining in lung from transgenic hACE2 mice upon SARS-CoV-2 (1 × 105 TCID50/mL) infection for 72 hr. Scale bar, 50 μm. b, Area of ACE2 and TOLLIP colocalization. c, Lysates of Calu-3 cells transfected with scramble or TOLLIP-specific siRNA treated with SARS-CoV-2 (MOI = 0.5) for indicated time points. The protein was harvested

for immunoblot analysis. d, Calu-3 cells were transfected with scramble or TOLLIP-specific siRNAs treated with SARS-CoV-2 (MOI = 0.5) for indicated time points. Relative expression levels of selected genes were measured by qPCR. e, Dot-plot visualization of enriched GO terms showing the enriched genes up-regulated by SARS-CoV-2 infection with or without 2-D08 (100 μM) treatment comparing with negative control. Calu-3 cells were infected SARS-CoV-2 at MOI = 0.5 for 24 hr. f, Heatmap indicating the expression levels of DEGs up-regulated by SARS-CoV-2 infection with different treatments, and the genes belonging to GO annotations for cytokine activity and chemokine activity (GO: 0005125 and GO: 0008009). Microarray analysis for total RNA was performed for SARS-CoV-2-infected Calu-3 cells together with or without 2-D08 treatment. g, IGV browser tracks showing the RNA-seq signals of selected genes in Calu-3 cells at indicated time points post infection with 2-D08 treatment. Data in (b) is expressed as means ± SD of 5 images. Data in (d) is expressed as means ± SEM of at least three independent experiments. ***p < 0.001 (two-tailed Student's t-test). For data in (c), similar results were obtained by three independent biological experiments.

## Supplementary Files

This is a list of supplementary files associated with this preprint. Click to download.

- Extendeddata.doc
- SupplementaryTable1.xlsx